



Adsorption of methyl violet dye from wastewater using poly(methacrylic acid-co-acrylamide)/bentonite nanocomposite hydrogels

Hamid Safarzadeh¹ · Seyed Jamaledin Peighambaroust² · Seyed Hamed Mousavi¹ · Reza Mohammadi³ · Seyed Hadi Peighambaroust⁴

Received: 30 September 2021 / Accepted: 21 February 2022 / Published online: 8 March 2022
© The Polymer Society, Taipei 2022

Abstract

In this study, nanocomposite hydrogels of poly(methacrylic acid-co-acrylamide) (Poly(MAA-co-AAm)) containing different weight percent bentonite clay nanoparticles (0, 5, 10, and 15 wt. %) were used to remove methyl violet (MV) dye. FTIR, SEM, TGA, and XRD were used to analyze the properties of adsorbents. Results showed that bentonite nanoparticles were successfully distributed in the hydrogel system. Bentonite nanoparticles at 10 wt. % gave the maximum MV dye adsorption efficiency. The highest adsorption was obtained at a pH of 5, an adsorbent dosage of 1.5 g/L, a temperature of 25 °C, a contact time of 60 min, and a pollutant concentration of 10 mg/L. In thermodynamics studies, a negative values of Gibbs free energy (ΔG°) indicating that the adsorption process was spontaneous. In addition, Poly(MAA-co-AAm) hydrogels and Poly(MAA-co-AAm)/bentonite nanocomposite hydrogels gave the adsorption enthalpy (ΔH°) of -61.24 and -36.14 kJ/mol which shows that the adsorption process is exothermic in the temperature range 25–45 °C using both adsorbents. Langmuir isotherm model was successfully applied in describing the equilibrium behavior of the adsorption process. The kinetic study showed that the pseudo-second-order model was more successful in describing the kinetic behavior of the adsorption process than pseudo-first-order and Elovich models. Poly(methacrylic acid-co-acrylamide) and poly(methacrylic acid-co-acrylamide)/bentonite adsorbents gave the α parameter values of 0.4276 and 22.15 mg.(g.min)⁻¹, respectively indicating the high adsorption capacity of these adsorbents.

Keywords Methacrylic acid-co-acrylamide copolymer · Nanocomposite hydrogel · Adsorption · Methyl Violet

Introduction

Water pollution from the improper discharge of industrial dyes originated from various industries such as textile, leather, paper, plastic, tanning, etc. is a very serious environmental concern, which threaten the living organisms and ecosystem [1, 2], thus, they have to be removed from wastewater streams before entering to the environment. Dyes are of major classes of polluting substances [3, 4] that are divided into cationic and anionic types [5, 6]. The annual production of industrial dyes is estimated to be 10,000 tons, of which about 1 to 10 percent of is being discharged to the environment [7]. Due to their complex structure, chemical dyes cause pollution in the environment and harm humans, animals and other living organisms, especially aquatic animals [8, 9]. Dyes are aromatic substances that have a high solubility in water, so they are easily dispersed in water and trap hydrogen molecules [10]. These pollutants are structurally divided into three categories: cationic, anionic, and non-ionic. Cationic dyes have more destructive effects than other

✉ Seyed Jamaledin Peighambaroust
j.peighambaroust@tabrizu.ac.ir

✉ Seyed Hamed Mousavi
mhmousavi@ut.ac.ir

¹ Separation Processes & Nanotechnology Lab, Faculty of Caspian, College of Engineering, University of Tehran, Tehran, Iran

² Faculty of Chemical and Petroleum Engineering, University of Tabriz, 5166616471 Tabriz, Iran

³ Polymer Research Laboratory, Department of Organic and Biochemistry, Faculty of Chemistry, University of Tabriz, Tabriz, Iran

⁴ Department of Food Science, College of Agriculture, University of Tabriz, 5166616471 Tabriz, Iran

dye pollutants. Most of them release into surface waters by the textile industry [11]. Malachite Green (MG) with the chemical formula of $C_{23}H_{26}ClN_3$ is a cationic dye with a molar mass of 393.94 g/mol. MG is one of the dyeing products of aniline. In various industries such as the production of paint, paper, clothing, textiles, and printing presses, the pollution of the aquatic environments can be seen due to the release of dye pollutants. Among these, textiles play a major role in polluting the aquatic environment of the planet because about 15% of the dye used in textile factories is disposed directly to the wastewaters that are released into surface waters [12, 13]. Complete removal of dyes from the wastewater streams is a challenging issue because of their longer stability in the environment. In previous studies various techniques such as electrochemical, ion exchange, catalysis, deformation and adsorption have been suggested to remove the dyes from aqueous solutions [14, 15]. In the adsorption process, a variety of natural and synthetic adsorbents such as chitosan, alginate, activated carbon, algae, etc. can be used. Among these, natural adsorbents have a high priority due to their availability as well as their reversibility and biodegradability. The presence of carboxyl, amine, and hydroxyl functional groups on the surface of the adsorbents are important factors in increasing the adsorption of pollutants [16, 17]. Water treatment systems based on hydrogel show the potential of efficient adsorption due to the three-dimensional network of polymer chains and hydrophilic nature of hydrogels [18]. In addition, hydrogels are cheap, non-toxic, chemically and physically stable, they form a good polymer network with a good ability to be recycled [19, 20]. Hydrogels exhibit a high adsorption affinity to remove different chemicals from aqueous solutions even at lower concentrations, which makes them important for widespread use in environmental applications [21, 22]. Numerous substances including natural polymers (chitin, chitosan, carboxymethyl cellulose, etc.), agricultural wastes, silicate layers such as mineral clays and activated carbon are used as a sorbent to remove some chemicals from wastewater [23]. Most of these materials are cheap, biocompatible and abundant having good mechanical and chemical properties enabling them to be used for wastewater treatment [24]. In general, all soils have a high swelling in the aqueous medium. There is no exception for Bentonite as a mineral material to this rule and due to the presence of van der Waals force in its structure, after adsorbing water, its volume reaches six times its original volume [25, 26]. Bentonite with overall formula $Al_2H_2Na_2O_{13}Si_4$ possesses a large surface area and cation-exchange ability making it suitable to remove organic dyes from wastewater [27, 28]. Of course, it should be noted that in clays with high water adsorption, the structure of this mineral is two quadrilateral layers of silica and one octahedral layer of alumina. By replacing silica (in the quadrilateral layer) with magnesium and divalent iron (in the octahedral layer), different groups are formed [29, 30]. The aim of this study was to synthesize and describe poly nanocomposite hydrogels (MAA-co-AAm)/bentonite as a biodegradable

adsorbent, inexpensive and effective in adsorbing methyl violet dye. Different techniques such as FTIR, TGA, SEM, and XRD were applied to specify the hydrogels' structure. Adsorption parameters including process temperature, time, the concentration of dye, adsorbent dosage and pH were studied. Mathematical models of Langmuir, Freundlich, Dubinin-Radushkevich (D-R) and Temkin isotherm were used to describe the equilibrium behavior of the adsorption process. Also, to study the kinetic behavior of the process, common models such as pseudo-first-order, pseudo-second-order, and Elovich were used. In addition, the thermodynamic behavior of traditional hydrogels was evaluated. In this study, the effect of operating conditions including pH, temperature, contact time, and initial MV concentration on the adsorption performance will be studied that is a need for optimization of the operating conditions. Also, the thermodynamic adsorption parameters of synthesized hydrogel samples were investigated for this adsorption process and changes in Gibbs free energy and entropy of the adsorption will be estimated at different temperatures. These thermodynamic data for the system of this grafted hydrogel composite as an adsorbent and MV as an adsorbent were never reported similarly by any scholars.

Materials and methods

Materials

Methacrylic acid (MAA) and acrylamide (AAm) monomers and methyl violet (MV) dye ($\lambda_{max} = 582$ nm) were purchased from Merck (Darmstadt, Germany). Potassium persulfate was obtained from Samchun (Seoul, South Korea). N,N'-Methylenebisacrylamide (MBA) and bentonite were purchased from Sigma Aldrich (Munich, Germany).

Synthesis of poly(MAA-co-AAm)/Bentonite nanocomposite hydrogels

Poly(MAA-co-AAm) and poly(MAA-co-AAm)/Bentonite nanocomposite hydrogels were prepared using free radical polymerization. For copolymerization of monomers in hydrogel synthesis, 5 ml MAA were poured in a three-necked flask equipped with nitrogen gas inlet–outlet, mechanical stirrer and a thermometer. Bentonite in a concentration of 0–15 wt. % was dispersed in 2 g of AAm and 10 mL of deionized water, and the mixture was sonicated for 20 min at 25 °C to fully disperse the nanoclay in the AAm solution. A mixture of bentonite, AAm and N,N'-Methylenebisacrylamide (MBA) as a crosslinker were added to the flask and heating was continued to 70 °C for 30 min. To produce free radicals potassium persulfate (as an initiator) was then added to the above mixture under nitrogen gas. The first signs of gel formation appeared after 20 min. The

reaction was performed for a total time of 3 h to complete the polymerization process. The obtained nanocomposite hydrogels were further purified to remove the non-reactive monomers by deionized water washing for several times. The obtained adsorbents (nanocomposite hydrogels) were let to dry out gently at 55 °C for 48 h followed by pulverization to pass through a sieve with 250–500 µm mesh size. Poly(MAA-co-AAm) hydrogel without bentonite nanoclay were synthesized according to the above-mentioned procedure for comparison purpose.

Characterization method

The chemical structure of monomers (MAA and AAm), bentonite nanoclay, poly(MAA-co-AAm) and poly(MAA-co-AAm)/bentonite nanocomposite hydrogels were examined using FTIR spectroscopy (Tensor 27, Broker, Germany) in a scanning range of 400 to 4000 cm^{-1} . X-ray diffraction patterns were obtained using an X-ray diffractometer (Siemens S5000, Germany) according to method described previously [27]. SEM was applied to characterize the surface morphology of nanocomposite hydrogels according to the procedure described previously [24]. EDXA and dot-mapping (Microanalysis Oxford Instruments model 7718 INCA PentaFET) technique was used to determine the distribution of nanoclay at the cross-section of hydrogels. Thermogravimetric analysis (TGA) was conducted to evaluate the thermal stability of samples [31]. To study the adsorption capacity, MV-dye at different concentrations (10–100 $\text{mg}\cdot\text{L}^{-1}$ DW) was used. For this purpose, 0.05 g of dry hydrogel was added to 50 mL of MV-dye solution and magnetically stirred (800 rpm) for 60 min. After reaching equilibrium adsorption capacity (initial tests were performed at 25 °C, contact time of 60 min and weight of 1 $\text{g}\cdot\text{L}^{-1}$ of the adsorbent dosage), the solutions were filtered by centrifugation its dye content was measured by UV-Vis spectrophotometry. The adsorption capacity of the adsorbents at equilibrium (q_e , $\text{mg}\cdot\text{L}^{-1}$) and adsorption efficiency (R %) were calculated using Eqs. 1 and 2, respectively.

$$R(\%) = \frac{(C_0 - C_t)}{C_0} \times 100 \quad (1)$$

$$q_t = \frac{(C_0 - C_t)V}{m} \quad (2)$$

where, C_0 is the initial concentration of the contaminant, C_t is the final concentration, V is the volume of the solution used, and m ($\text{g}\cdot\text{L}^{-1}$) is amount of adsorbent used.

Swelling behavior of hydrogels

Swelling behavior of copolymer and nanocomposite hydrogel samples were investigated. For this purpose, 20 mg of

adsorbent was poured into 10 mL of DW and after one day (24 h), the solution was centrifuged. The adsorbent was separated from DW and weighed. The amount of adsorbent swelling ratio was calculated using Eq. (3) [24].

$$\text{Swelling Ratio} = \frac{(W_{\text{wet}} - W_{\text{dry}})}{W_{\text{dry}}} \quad (3)$$

where W_{wet} and W_{dry} are the wet and dry weights of the hydrogels, respectively.

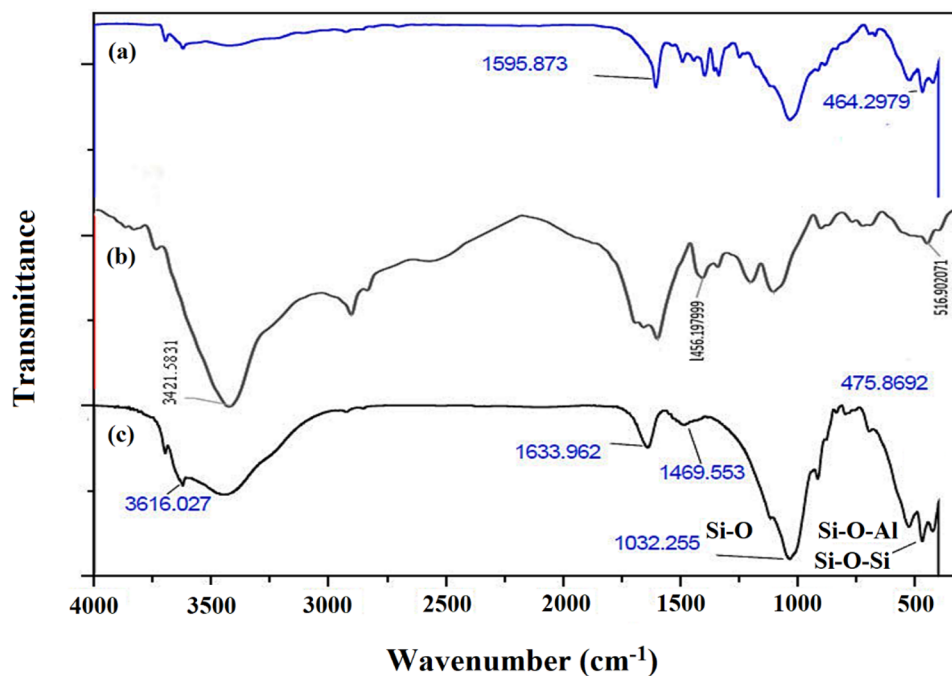
Results and Discussion

Properties of hydrogels

Figure 1a shows the FTIR spectra of the bentonite nanoparticles indicating characteristic peaks at wavenumber of 3616 cm^{-1} (corresponding to the tensile vibration of the hydrogen bonds), 1474 and 1596 cm^{-1} (indicating the bending of Nitrate-ions) [32]. The rest of the vibrations are in the range of 1000–1050 cm^{-1} due to the tension of the Si–O–C bond [33]. Figure 1b shows the FTIR spectra of poly(MAA-co-AAm) hydrogel after adsorption of the dye contaminant. The peaks at 1631 and 1699 cm^{-1} indicate the involvement of the carbonyl and vinyl groups of MAA monomer in the free radical polymerization. In addition, the peaks of 1728 and 1751 cm^{-1} are symmetrically bonded to carboxylate anions and C=O tensile vibrations in the monomers, respectively [34]. The absorption peaks at wavenumbers of 1648 and 1654 cm^{-1} were assigned to the C=C in MMA and AAm disappeared after polymerization. Figure 1c shows the FTIR spectra of poly(MAA-co-AAm)/bentonite nanocomposites after adsorption of MV dye. Compared to the shape of the copolymer hydrogel, the vibration distance was reduced, which indicates that the methyl violet (MV) dye was trapped in the pores of the nanocomposite. In addition, the increase in the transmission spectrum in 1653 cm^{-1} , which is related to the poly(MAA-co-AAm) bonds, indicates that these bonds are filled with dye contaminants. Finally, the peaks in the nanocomposite structure between 400–500 cm^{-1} are related to Si–O–Si and Si–O–Al bond tension [35].

Figure 2 shows the XRD patterns of bentonite nanoparticles, poly(MAA-co-AAm), and poly(MAA-co-AAm)/bentonite nanocomposite hydrogels. As shown in the figure, bentonite nanoclay shows many diffraction peaks due to the presence of different crystalline phases. The distinct peak at $2\theta = 5\text{--}10^\circ$ (specified in $2\theta = 5.7^\circ$) related to the basal-spacing (d_{001}) for layered gallery structure of bentonite nanoclay. From Bragg's equation for layered silicates such as bentonite nanoclay, the d_{001} is calculated as 1.55 nm. For poly(MAA-co-AAm) and poly(MAA-co-AAm)/bentonite

Fig. 1 FTIR results for **a**) bentonite **b**) poly(MAA-co-AAm) hydrogel **c**) poly(MAA-co-AAm)/bentonite nanocomposite hydrogel



nanocomposite hydrogels, this distinct peak hasn't appeared which can be due to the complete disaggregation of the bentonite silicate layers during the formation of the nanocomposite structure. This means the complete dispersion of single layers of clay into polymeric matrix occurred. In this case, the exfoliated structure for the resulting nanocomposite is obtained. The XRD results showed that the formation of a layer structure (exfoliation) in the obtained nanocomposite structure, indicates the proper distribution of nanoclay particles in the polymer matrix, which is a reason to increase the resistance and thermal properties of nanocomposite hydrogel. Also, in the poly(MAA-co-AAm)/bentonite nanocomposite hydrogel XRD pattern, some peaks in $2\theta = 12.5$, 16 , and 22° are observed which indicating the amorphous structure of copolymer samples [36].

Figure 3 shows the TGA curves of poly(MAA-co-AAm) and poly(MAA-co-AAm)/bentonite nanocomposite hydrogels and the detailed TGA analysis results are shown in Table 1. Usually, TGA analysis was performed to investigate the thermal stability behavior of poly(MAA-co-AAm) and poly(MAA-co-AAm)/bentonite nanocomposite hydrogels. The results of TGA analysis showed that the weight loss of copolymer and nanocomposite hydrogel samples was done in three stages. The first stage of weight loss occurred in the range of 50 – 150°C temperature, which could be due to water loss in the sample by evaporation. It is noteworthy to mention that at this stage, the weight loss of the nanocomposite sample is more than the copolymer hydrogel sample and this is due to a large number of water molecules in the hydrogel nanocomposites structure [37]. In the 2nd degradation stage,

Fig. 2 X-ray diffraction results (XRD) of bentonite, poly(MAA-co-AAm), and poly(MAA-co-AAm)/bentonite nanocomposites

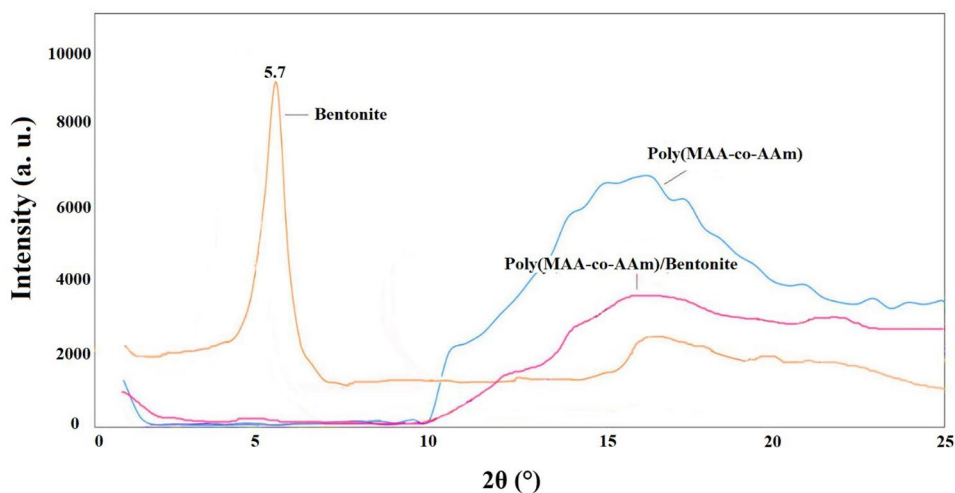
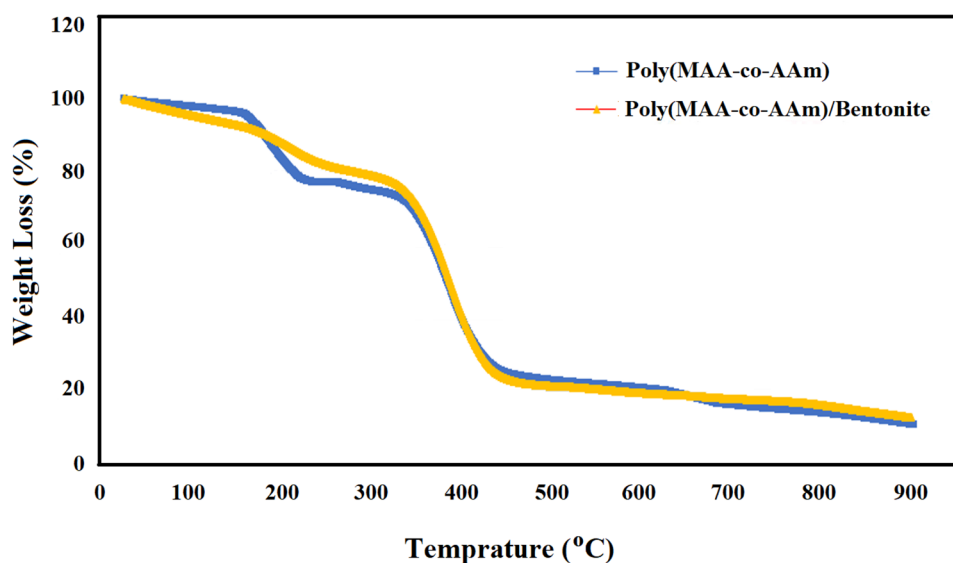


Fig. 3 Comparison of TGA analysis results of poly(MAA-co-AAm) and poly(MAA-co-AAm)/bentonite nanocomposite hydrogels



weight loss of about 7.4 wt. % at the temperature range of 168–208 °C is related to the breaking of C–O–C bonds in the chains of methacrylic acid and the resulting hydrogels [32, 34]. The another stage of weight loss took place in the range of 200–450 °C temperature, where the hydrogels lost a significant part of their weight, which could be related to the destruction of acrylamide bonds as well as the decomposition of excellent monomer compounds. Also at this stage, the C–H bond of methacrylic acid, which is the dominant monomer of the hydrogel, is decomposed. The final weight loss can be due to the decomposition and destruction of the structure of the mentioned materials, which at this stage we see a slight weight loss. As shown in Fig. 3, the addition of bentonite nanoparticles increases the thermal stability of the nanocomposite. In addition, a comparison of the nanocomposite sample with the sample without nanoclay shows that the addition of bentonite nanoclay to the polymeric hydrogel caused a significant increase in the temperature of the nanocomposite during the heating steps. This result may be due to the exfoliated structure that creates strong hydrogen bond

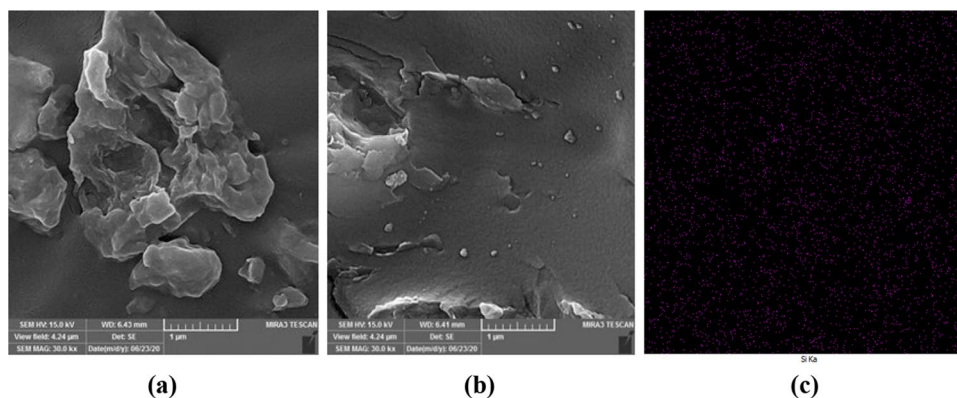
interactions with methacrylic acid and acrylamide monomers, evaporating water molecules, destroying the chains and opening the nanocomposite layers.

In order to study morphology and changes in samples of poly(MAA-co-AAm) and poly(MAA-co-AAm)/bentonite nanocomposite hydrogels before and after the methyl violet dye adsorption process, SEM–EDX and dot-mapping analysis were used. Figure 4 shows the SEM micrographs for poly(MAA-co-AAm) and poly(MAA-co-AAm)/bentonite nanocomposite hydrogels in the dry state. In hydrogels, the amount of swelling depends on the porosity and the average size of the pores. Due to the presence of capillary forces, water is distributed through the pores. As shown in Fig. 4b the presence of bentonite nanoparticles increases the porosity of hydrogel and thus, increases the water permeability in the structure of hydrogels. Dot mapping results (Fig. 4c) show the cross-sectional distribution of Si element (purple dots) as a marker of nanoparticles. Figure 4a also showed a uniform distribution of nanoparticles in the microstructure of nanocomposite hydrogels

Table 1 Detailed TGA analysis results

Stage of Weight Loss	Weight Loss (%)	Range of Weight Loss (°C)	Reason
First for Copolymer	4.2	50–150	water loss
Total for Nanocomposite	5.7		
Second for Copolymer	7.4	168–208	breaking of C–O–C bonds
Total for Nanocomposite	4.1		
Third for Copolymer	52.4	250–450	destruction of acrylamide bonds and monomer compounds
Total for Nanocomposite	51.9		
Forth for Copolymer	25.26	Over 450	decomposition of the materials structure
Total for Nanocomposite	23.46		
Total for Copolymer	89.26	0–900	–
Total for Nanocomposite	85.16		

Fig. 4 SEM images of **a**) poly(MAA-co-AAm) hydrogel (1 μm), **b**) poly(MAA-co-AAm)/bentonite nanocomposite hydrogel (1 μm), and **c**) dot-mapping of nanocomposite hydrogel for same resolution (1 μm)



confirming that clay nanoparticles were not accumulated in the matrix. Also, after the adsorption process of MV-dye, the pores and surface roughness of the nanocomposite were almost saturated, which can be due to the filling of the pore by dye molecules.

The effect of different parameters on the adsorption performance

Weight concentration of nanoparticles

Figure 5a shows effect of weight percent of nanoparticles on dye adsorption efficiency. A lower dye adsorption was observed at either low (2.5 wt. %) or high (15 wt. %) concentrations of nanoparticles. The highest dye adsorption of 96% was obtained at a nanoparticle weight percent range of 7.5–12.5 (wt %). It is known that with increasing the weight percentage of bentonite nanoparticles inside the hydrogel, due to the increase of active sites and effective surface, the amount of dye adsorption increased sharply and when the amount of bentonite nanoparticles reached to 12.5 wt. %, due to the accumulation of these nanoparticles inside the hydrogel, the dye adsorption decreases because in this weight percentage, the active sites available for the adsorption process are reduced.

Effect of pH

The initial pH of the medium is an important factor of the adsorption process that affects adsorbent surface ionization and charge [38]. Figure 5b shows the effect of initial pH (in a range of 3–10) on the efficiency of dye adsorption for Poly(MAA-co-AAm) and Poly(MAA-co-AAm)/bentonite nanocomposite hydrogels. First, the adsorption efficiency of Poly(MAA-co-AAm)/bentonite was higher than that of Poly(MAA-co-AAm) hydrogels at all pH ranges tested. Second, either at lower ($\text{pH} < 4$) or higher ($\text{pH} > 9$) pH values,

the adsorption efficiency was significantly reduced. A highest adsorption rate of 94 and 90% was obtained at $\text{pH} = 7$ for Poly(MAA-co-AAm)/bentonite and Poly(MAA-co-AAm) hydrogels, respectively. There are repulsive electrostatic forces between the surface of adsorbent and the dye molecules originated from H^+ ions in acidic pH, and OH^- ions in alkaline pH, which reduce the adsorption efficiency [39, 40].

Adsorbent dose

The adsorbent dose is another important parameter that affects the adsorption efficiency of contaminants [41]. In this study, the adsorption capacity of Poly(MAA-co-AAm) and Poly(MAA-co-AAm)/bentonite nanocomposite hydrogels was evaluated at an adsorbent dose range of 0.5–4 g.L^{-1} , an initial dye concentration of 10 mg.L^{-1} , an initial pH of 7, and a contact time of 60 min. As can be seen from Fig. 5c, the adsorption efficiency of Poly(MAA-co-AAm)/bentonite nanocomposite hydrogel was higher than that of Poly(MAA-co-AAm) hydrogel at all adsorbent dosages tested. With increasing the adsorbent dose, a favorable increase in the adsorption efficiency for both types of hydrogels was observed. This can be explained by an increased contact surface of the adsorbents, which facilitates the adsorption process at a higher concentration. According to the results, with increasing the adsorbent dose from 0.5 to 1.5 g.L^{-1} , the adsorption efficiency of the dye was increased. Dosage higher than 1.5 g.L^{-1} did not significantly change the adsorption efficiency of both adsorbent types. This could be due to the reduction of dye concentration in aqueous solution and reduction of active ingredient [42].

Effect of dye concentration

The concentration of pollutants is also an important factor in the adsorption process because it acts as a driving force of mass transfer between the adsorbent (solid phase) and the

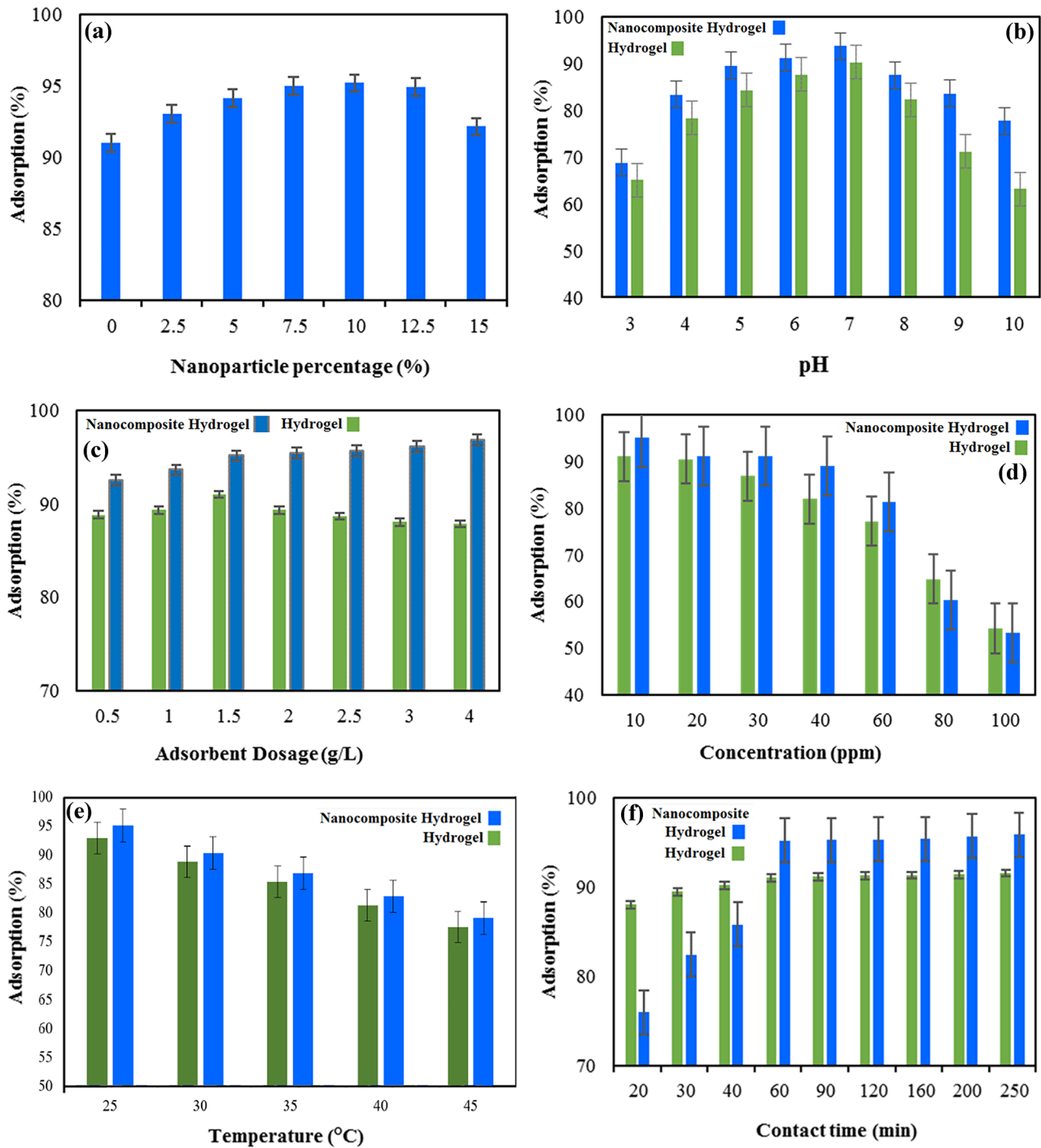


Fig. 5 a) Effect of nanoparticle wt. %, b) pH, c) adsorbent dosage, d) the initial concentration of dye (MV), e) contact time, and f) temperature on adsorption efficiency of poly(MAA-co-AAm) and poly(MAA-

co-AAm)/bentonite nanocomposite hydrogels. Data are mean of triplicate measurements. Error bars indicate the standard deviation

aqueous phase [43]. Figure 5d shows the effect dye concentration on the efficiency of the adsorption process. Increasing the concentration significantly decreased the adsorption efficiency for both types of adsorbents. At low dye concentrations

(i.e., 10 mg.L^{-1}), the intermolecular bonds of the dyes could be weak, while at high concentrations (i.e., 100 mg.L^{-1}) the active sites on the adsorbent surface are completely saturated leaving extra dye molecules unadsorbed [44–46].

Effect of temperature

Temperature influences the kinetic energy of adsorbent molecules, and thereby, could affect the efficiency of the adsorption process [24]. The effects of temperature change in the range of 25–45 °C on the adsorption efficiency are shown in Fig. 5e. Increasing the temperature could enhance the mobility of the hydrogel side groups causing the adsorbed dye molecules to be separated from the hydrogel structure and reduce the adsorption rate. This process indicates that the adsorption reaction is exothermic. The highest adsorption rate (95%) was obtained at a temperature of 25 °C.

Contact time

The efficiency of adsorption at time intervals of 20–250 min was evaluated considering a pH of 7, and an adsorbent dose of 1.5 g.L⁻¹. Figure 5f shows that the adsorption of dyes was faster in the beginning of the process; however, the adsorption rate reached to a plateau after 60 min. In the beginning, there are unoccupied surfaces that are active to absorb the dye. Upon increasing contact time, those active sites on the adsorbent molecules become saturated, which this leads to a reduction in the adsorption rate. According to the results, the optimal time for adsorption of dye with an initial concentration of 10 mg.L⁻¹ was obtained at 60 min.

Adsorption isotherm models

To evaluate the adsorption behavior of dye contaminants using two types of adsorbent hydrogels the Langmuir [47], Freundlich [23], Dubinin-Radushkevich (D-R) [48], and Temkin [27] isotherm models were used according to following equations.

$$\text{Langmuir : } q_e = \frac{q_m \cdot k_1 \cdot C_e}{1 + k_1 \cdot C_e}, \quad R_L = \frac{1}{1 + K_L + C_0} \quad (4)$$

$$\text{Freundlich : } q_e = k_f C_e^{1/n} \quad (5)$$

$$\text{D - R : } q_e = q_m \cdot \exp(-\beta \epsilon^2), \quad \epsilon = RT \text{Ln} \left(1 + \frac{1}{C_e} \right) \quad (6)$$

$$\text{Temkin : } q_e = B \text{Ln}(A \times C_e), \quad B = \frac{RT}{b_T} \quad (7)$$

In these equations q_m shows the maximum dye absorption capacity (mg.g⁻¹), K_F and n are Freundlich constants, ϵ represents Polanyi coefficient, K_L is Langmuir constant, A (g⁻¹) and b_T (kJ.mol⁻¹) are the Temkin constants, β is the activity coefficient (mol².J⁻²), R is the universal gas constant and T is the absolute temperature (K). [49–51]. Table 1 shows the constants and parameters of the models. In addition, R_L is a dimensionless parameter in Langmuir model, which shows the type of adsorption process. The value of $R_L > 1$ indicates undesirable, $R_L = 1$ shows linear, $R_L = 0$ represents irreversible, and $0 < R_L < 1$ indicates desirable adsorption processes. As shown in Table 2, a value range 0–1 was obtained for R_L parameter using for both adsorbent types of showing that the adsorption process was optimal [23]. The adsorbents synthesized in the present study showed a highly potential in removal of MV dyes compared to other adsorbents of researchers’ studies (Table 3). By drawing a linear isothermal shape, a constant can be obtained [27]. The isotherm models using synthesized adsorbents showed nonlinear relationship (Fig. 6).

Using Langmuir model, the correlation coefficient (R^2) was 0.9965 for Poly(MAA-co-AAm) hydrogel and 0.9986 for Poly(MAA-co-AAm)/Bentonite hydrogel adsorbents. These values were significantly higher than those of other models. In addition, the n parameters obtained using Poly(MAA-co-AAm) and Poly(MAA-co-AAm)/Bentonite hydrogels were 2.75 and 3.27, respectively, indicating that the MV dye adsorption process using these types of adsorbents are both optimal and physical. The A_T and b_T parameters determined by the Temkin model showed that the

Table 2 Equilibrium constants and parameters from adsorption process of MV dye

Hydrogel sample	Langmuir	Freundlich	Temkin	Dubinin–Radushkevich (D-R)				
Poly(MAA-co-AAm)	q_m	137.037	n	2.75	B	6.612	E	0.176
	k	0.201	k	10.69	A_T	5.79	q_m	150.45
	R_L	0.014–0.488	R^2	0.8781	R^2	0.9351	β	4×10^{-6}
	R^2	0.9965					R^2	0.9214
Poly(MAA-co-AAm)/bentonite Nanaocomposite	q_m	149.32	n	3.27	B	8.077	E	0.372
	k	0.374	k	8.26	A_T	2.34	q_m	174.11
	R_L	0.009–0.338	R^2	0.9287	R^2	0.9844	β	9×10^{-7}
	R^2	0.9986					R^2	0.9398

Table 3 Comparison of adsorption capacity of Poly(MAA-co-AAm) hydrogel and Poly(MAA-co-AAm)/bentonite nanocomposite hydrogel with other adsorbents in adsorption of MV dye from aqueous solution

Adsorbent	q_e (mg/g)	Reference
Activated carbon (laboratory grade)	12.552	[42]
NaOH-treated Sargassum fluitans	99.83	[43]
BDH activated carbon	6.56	[44]
Neem sawdust	4.354	[45]
CMC-g-P(AAm)/MMT	172.4	[22]
Gum xanthan-psyllium-cl poly(acrylic acid-coitaconic)	1.641	[46]
PANI-ZrPB	56	[47]
CMC-g-P(MMA)/Cloisite 30B	140.845	[24]
BCMFCr(VI)	178.57	[40]
Poly(MAA-co-AAm)	137.037	This work
Poly(MAA-co-AAm)/bentonite	149.32	This work

interaction between MV dye and adsorbent surface is weak. Also, the D-R isotherm model showed a value of 8 kJ.mol^{-1} for the $E = \frac{1}{\sqrt{2\beta}}$ parameter which indicates the physicality of the hydrogels' adsorption process [24].

Thermodynamic study

Thermodynamic parameters such as enthalpy (ΔH°), entropy (ΔS°) and Gibbs free energy (ΔG°) were calculated according to Eqs. 8 and 9 [52–54].

$$\Delta G = -R T \text{Ln} (1000 \times K_D) \quad (8)$$

$$\text{Ln} (1000 \times K_D) = \frac{-\Delta H^\circ}{RT} + \frac{\Delta S^\circ}{R} \quad (9)$$

where, T is the absolute temperature (K), R is the universal constant of gases (8.314 J/mol.K) and K_D ($K_D = q_e/C_e$) is the equilibrium constant.

The values ΔH° and ΔS° are determined by the slope and width of $\text{Ln } K_D$ vs. $1/T$ in the diagram, respectively, which can be seen in Fig. 7, and the obtained parameters are summarized in Table 4. A negative value of ΔG° parameter for both types of adsorbents indicates that the MV-dye adsorption

process was successful and spontaneous. Moreover, negative values of ΔH° parameter for Poly(MAA-co-AAm) ($-61.24 \text{ kJ.mol}^{-1}$) and Poly(MAA-co-AAm)/bentonite ($-36.14 \text{ kJ.mol}^{-1}$) hydrogels showed that the adsorption process was exothermic (at a temperature range $25\text{--}45^\circ \text{C}$). The negative value of ΔS° also showed that the random collisions of dye molecules with the adsorbent surface increased during the adsorption process [24, 55].

Kinetics study

In this study, pseudo-first-order [56], pseudo-second-order [57], and Elovich [58] kinematic models were used to analyze experimental data according to Eqs. (10), (11) and (12), respectively.

$$q_t = q_e (1 - e^{-k_1 t}) \quad (10)$$

$$q_t = \frac{k_2 q_e^2 t}{1 + k_2 q_e t} \quad (11)$$

$$q_t = \frac{1}{\beta} \text{Ln} (\alpha \beta t) \quad (12)$$

where, q_t and q_e show the adsorption capacity at time t of dye per gram of dry adsorbent and the equilibrium adsorption capacity (mg.g^{-1}) respectively, k_1 and k_2 are the constants of adsorption rates (k_1 is constant adsorption rate (min^{-1}) and k_2 is the constant quasi-quadratic kinetic model rate (g.(mg.min)^{-1})), α and β are the initial absorbance (mg.(g.min)^{-1}) and the desorption constant (g.mg^{-1}) respectively, in Elovich kinetic model. The slope and cut of the log diagram ($q_e - q_t$) in front of t represent k_1 and q_e . In the same way, k_2 and q_e are calculated with graph t/q_t versus t . Correlation coefficients were calculated and obtained from the analysis of experimental data using three kinetic models used in the study [59, 60]. Equation (10) for the pseudo-first-order and Eq. (11) for the pseudo-second-order were used to study the kinetics linearly. The relation between kinetic parameters using both types of adsorbents are shown in Fig. 8. The kinetic parameters of the adsorption of MV-dye using both types of adsorbents are shown in Table 5. As can be seen from Fig. 8 and Table 5,

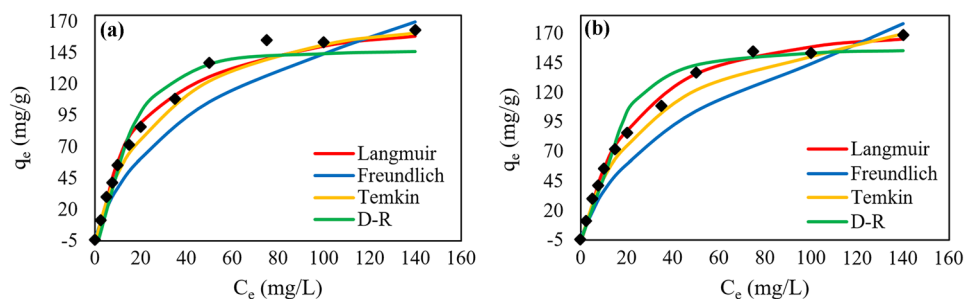
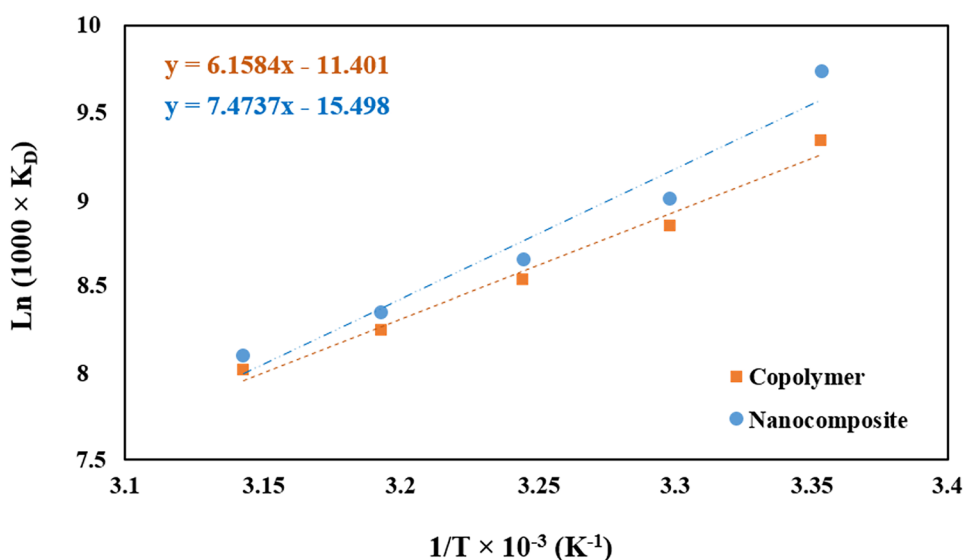
Fig. 6 Linear relationship of Langmuir, Freundlich, Temkin, and D-R isotherm models for the adsorption MV dye from aqueous solution using Poly(MAA-co-AAm) hydrogel and Poly(MAA-co-AAm)/bentonite nanocomposite hydrogel

Fig. 7 Relation of $\ln K_D$ vs. $1/T$ to determine thermodynamic parameters



and the value of R^2 , the pseudo-second-order for Poly(MAA-co-AAm) and Poly(MAA-co-AAm)/bentonite nanocomposite hydrogels showed better and closer results to experimental results. In general, the quasi-quadratic kinetic model has a higher correlation and absorption coefficient compared to other kinetic models. By examining and considering the values of the q_t and k_2 parameters as well as matching the

data with the quasi-quadratic kinetic model, the MV dye adsorption process may be followed by a combined chemical and physical mechanism. Parameter values of α for MV dye adsorption process were calculated using Poly(MAA-co-AAm) and Poly(MAA-co-AAm)/Bentonite hydrogels at $0.4276 \text{ mg.g}^{-1}.\text{min}$ and $22.15 \text{ mg.g}^{-1}.\text{min}$. These results indicate a high adsorption value of nanocomposites.

Table 4 Thermodynamic constants and parameters for the adsorption process of MV dye using Poly(MAA-co-AAm) hydrogel and Poly(MAA-co-AAm)/Bentonite nanocomposite hydrogel

Adsorbent)	T (°C)	ΔG° (KJ/mol)	ΔH° (KJ/mol)	ΔS° (J/mol.K)
Poly(MAA-co-AAm) Hydrogel	25	-23.136	-51.20	-94.78
	30	-22.287		
	35	-21.868		
	40	-21.463		
	45	-21.198		
Poly(MAA-co-AAm)/bentonite Nanocomposite Hydrogel	25	-22.132	-62.136	-128.85
	30	-22.69		
	35	-22.168		
	40	-21.727		
	45	-21.431		

Fig. 8 Nonlinear relationship of kinetic models to determine the kinetic parameters of the adsorption process MV dye using Poly(MAA-co-AAm) hydrogel and Poly(MAA-co-AAm)/bentonite nanocomposite hydrogels

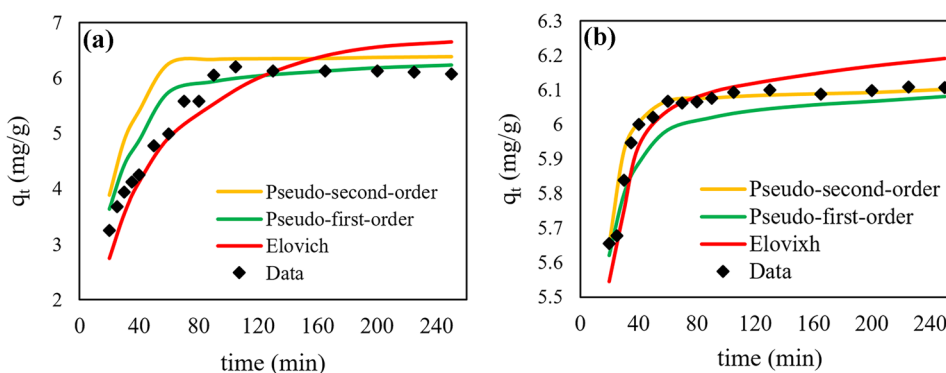


Table 5 Kinetic constants and parameters determined for the adsorption process of MV dye

Hydrogel sample	Pseudo-first-order Model		Pseudo-second-order Model		Elovich Model	
Poly(MAA-co-AAm) Hydrogel	q_t	5.33	q_t	18.699	α	0.4276
	K_1	0.012	K_2	0.341	β	0.219
	R^2	0.925	R^2	0.932	R^2	0.876
Poly(MAA-co-AAm)/bentonite Nanaocomposite Hydrogel	q_t	6.069	q_t	17.639	α	22.15
	K_1	0.165	K_2	0.433	β	0.436
	R^2	0.816	R^2	0.977	R^2	0.9042

Conclusions

Dyes and pigments are the main pollutants in wastewater streams of various industries. Poly(MAA-co-AAm) hydrogels and Poly(MAA-co-AAm)/bentonite adsorbents were used to remove MV-dye from aqueous solution. Amide and carboxylate functional groups were characterized by FTIR in the structure of adsorbents that could be important for the adsorption process. SEM confirmed the presence of numerous surface pores at in the surface of adsorbents that possibly favors the adsorption efficiency of MV-dye. The Langmuir model was found to be more capable in interpreting equilibrium behavior than other models. In addition, the values obtained from the parameters R_L , n and E of isothermal models, showed that the dye adsorption process of MV dye is physical and desirable. Temkin isotherm model (A_T and b_T parameters) showed a weak interaction of the adsorbent surface with the MV-dye. The determined kinetic data showed a good agreement with the quasi-second-order kinetic model and the latter had a better correlation coefficient and higher adsorption capacity than those of other models. By examining and considering the values of the q_t and k_2 parameters as well as matching the data with the quasi-quadratic kinetic model, the MV dye adsorption process may be followed by a combined chemical and physical mechanism. The thermodynamic study showed that the adsorption process was spontaneous and exothermic.

Declarations

Conflict of interest statement This work was conducted in the absence of any commercial or financial relationships that could be construed as a potential conflict of interest. Thus, the authors declare no conflict of interest.

References

- Mittal H, Babu R, Alhassan SM (2020) Utilization of gum xanthan based superporous hydrogels for the effective removal of methyl violet from aqueous solution. *Int J Biol Macromol* 143:413–423
- Wadhwa P, Jindal R, Dogra R (2019) Synthesis of semi interpenetrating network hydrogel [(GrA-Psy)-cl-Poly (AA)] and its application for efficient removal of malachite green from aqueous solution. *Polym Eng Sci* 59:1416–1427
- Eskhan A, Banat F, Selvaraj M, Abu Haija M (2019) Enhanced removal of methyl violet 6B cationic dye from aqueous solutions using calcium alginate hydrogel grafted with poly (styrene-co-maleic anhydride). *Polym Bull* 76:175–203. <https://doi.org/10.1007/s00289-018-2378-y>
- Beyranvand NS, Samiey B, Tehrani AD, Soleimani K (2019) Graphene oxide–cellulose nanowhisker hydrogel nanocomposite as a novel adsorbent for methylene blue. *J Chem Eng Data* 64:5558–5570
- Sharma G, Kumar A, Sharma S, Ala'a H, Naushad M, Ghfar AA, Ahamad T, Stadler FJ (2019) Fabrication and characterization of novel Fe0@ Guar gum-crosslinked-soya lecithin nanocomposite hydrogel for photocatalytic degradation of methyl violet dye. *Sep Purif Technol* 211:895–908
- Gadisa BT, Appiah-Ntiamoah R, Kim H (2019) Amorphous iron sulfide nanowires as an efficient adsorbent for toxic dye effluents remediation. *Environ Sci Pollut Res* 26:2734–2746
- Foroutan R, Mohammadi R, Ramavandi B (2019) Elimination performance of methylene blue, methyl violet, and Nile blue from aqueous media using AC/CoFe₂O₄ as a recyclable magnetic composite. *Environ Sci Pollut Res* 26:19523–19539
- Foroutan R, Mohammadi R, Razeghi J, Ramavandi B (2019) Performance of algal activated carbon/Fe₃O₄ magnetic composite for cationic dyes removal from aqueous solutions. *Algal Res* 40:101509
- Munagapati VS, Yarramuthi V, Kim Y, Lee KM, Kim DS (2018) Removal of anionic dyes (Reactive Black 5 and Congo Red) from aqueous solutions using banana peel powder as an adsorbent. *Eco-toxicol Environ Saf* 148:601–607
- Cheng K, Huang C, Wei Y, Hsu S (2019) Novel chitosan – cellulose nano fiber self-healing hydrogels to correlate self-healing properties of hydrogels with neural regeneration effects. *NPG Asia Mater* 11:25
- Cheng-Wei T, Fang-Chang T, Jem-Kun C, Huei-Ping W, Rong-Ho L, Jiawei Z, Tao C, Chung-Chi W, Chih-Feng H (2020) Preparations of Tough and Conductive PAMPS/PAA Double Network Hydrogels Containing Cellulose Nanofibers and Polypyrroles. *Polymers* 12(12):2835
- Chadi A, Olasupo A, Yani N, Saime W, Ngah W, Mohd B (2021) Journal of Environmental Chemical Engineering Comparative removal of malachite green dye from aqueous solution using deep eutectic solvents modified magnetic chitosan nanoparticles and modified protonated chitosan beads. *J Environ Chem Eng* 9(5):106281
- Li Z et al (2020) Removal of malachite green dye from aqueous solution by adsorbents derived from polyurethane plastic waste. *Biochem Pharmacol*, no. August, p 104704
- Mallakpour S, Tabesh F (2019) Tragacanth gum based hydrogel nanocomposites for the adsorption of methylene blue: Comparison

- of linear and non-linear forms of different adsorption isotherm and kinetics models. *Int J Biol Macromol* 133:754–766
15. Mittal H, Morajkar PP, Al Alili A, Alhassan SM (2020) In-situ synthesis of ZnO nanoparticles using gum arabic based hydrogels as a self-template for effective malachite green dye adsorption. *J Polym Environ* 28:1637–1653
 16. Tsai Y, Theato P, Huang C, Hsu S (2020) A 3D-printable, glucose-sensitive and thermoresponsive hydrogel as sacrificial materials for constructs with vascular-like channels. *Appl Mater Today* 20:100778
 17. Che-Hao W, Cheng-Wei T, Junko A, Jiawei Zhang TC, Chung-Chi W, Chih-Feng H (2020) Mechanochromic Double Network Hydrogels as a Compression Stress Sensor. *Polym Chem* 11(40):2020
 18. Thakur S, Verma A, Sharma B, Chaudhary J, Tamulevicius S, Thakur VK (2018) Recent developments in recycling of polystyrene based plastics. *Curr Opin Green Sustain Chem* 13:32–38
 19. Kaur K, Jindal R (2019) Comparative study on the behaviour of Chitosan-Gelatin based Hydrogel and nanocomposite ion exchanger synthesized under microwave conditions towards photocatalytic removal of cationic dyes. *Carbohydr Polym* 207:398–410
 20. Verma A, Thakur S, Mamba G, Gupta RK, Thakur P, Thakur VK (2020) Graphite modified sodium alginate hydrogel composite for efficient removal of malachite green dye. *Int J Biol Macromol* 148:1130–1139
 21. Rabipour M, Pour ZS, Sahraei R, Ghaemy M, Jazi ME, MIsna TE (2020) pH-Sensitive Nanocomposite Hydrogels Based on Poly (Vinyl Alcohol) Macromonomer and Graphene Oxide for Removal of Cationic Dyes from Aqueous Solutions. *J Polym Environ* 28:584–597
 22. Al-Aidy H, Amdeha E (2021) Green adsorbents based on polyacrylic acid-acrylamide grafted starch hydrogels: the new approach for enhanced adsorption of malachite green dye from aqueous solution. *Int J Environ Anal Chem* 101(15):2796–2816
 23. Pakdel PM, Peighambaroust SJ (2018) Review on recent progress in chitosan-based hydrogels for wastewater treatment application. *Carbohydr Polym* 201:264–279
 24. Sharma K, Kumar V, Kaith BS, Kumar V, Som S, Kalia S, Swart HC (2015) Synthesis, characterization and water retention study of biodegradable Gum ghatti-poly (acrylic acid-aniline) hydrogels. *Polym Degrad Stab* 111:20–31
 25. Kuo S, Chang F (2011) Progress in Polymer Science POSS related polymer nanocomposites. *Prog Polym Sci* 36(12):1649–1696
 26. Lu C, Kuo S, Huang C, Chang F (2009) Self-Assembled Fernlike Microstructures of Polyhedral Oligomeric Silsesquioxane / Gold Nanoparticle Hybrids. *J Phys Chem C* 113:3517–3524
 27. Pakdel PM, Peighambaroust SJ (2018) A review on acrylic based hydrogels and their applications in wastewater treatment. *J Environ Manage* 217:123–143
 28. Foroutan R, Peighambaroust SJ, Peighambaroust SH, Pateiro M, Lorenzo JM (2021) Adsorption of Crystal Violet Dye Using Activated Carbon of Lemon Wood and Activated Carbon/Fe₃O₄ Magnetic Nanocomposite from Aqueous Solutions: A Kinetic, Equilibrium and Thermodynamic Study *Mol* 26
 29. Xu H, Kuo S, Huang C, Chang F (2004) Characterization of Poly (vinyl pyrrolidone-co - isobutylstyryl polyhedral oligomeric silsesquioxane) nanocomposites. *J Appl Polym Sci* 91:2208
 30. Yen Y, Kuo S, Huang C, Chen J (2008) Miscibility and Hydrogen-Bonding Behavior in Organic / Inorganic Polymer Hybrids Containing Octaphenol Polyhedral Oligomeric Silsesquioxane. *J Phys Chem B* 112:10821–10829
 31. Peighambaroust SJ, Aghamohammadi-Bavil O, Foroutan R, Arsalani N (2020) Removal of malachite green using carboxymethyl cellulose-g-polyacrylamide/montmorillonite nanocomposite hydrogel. *Int J Biol Macromol* 159:1122–1131. <https://doi.org/10.1016/j.ijbiomac.2020.05.093>
 32. Moharrami P, Motamedi E (2020) Application of cellulose nanocrystals prepared from agricultural wastes for synthesis of starch-based hydrogel nanocomposites: Efficient and selective nano-adsorbent for removal of cationic dyes from water. *Bioresour Technol* 313:123661
 33. Abdolhosseinzadeh M, Peighambaroust SJ, Erfan-Niya H, Pakdel PM (2018) Swelling and auramine-O adsorption of carboxymethyl cellulose grafted poly (methyl methacrylate)/Cloisite 30B nanocomposite hydrogels. *Iran Polym J* 27:807–818
 34. da Silva RC, de Aguiar SB, da Cunha PLR, de Paula RCM, Feitosa JPA (2020) Effect of microwave on the synthesis of polyacrylamide-g-chitosan gel for azo dye removal. *React Funct Polym* 148:104491
 35. Wang G, Shen J, Liu S, Jiang C, Qin X (2019) Three-dimensional modeling and analysis of macro-pore structure of coal using combined X-ray CT imaging and fractal theory. *Int J Rock Mech Min Sci* 123:104082
 36. Nzioka AM, Kim M-G, Hwang H-U, Kim Y-J (2019) Kinetic study of the thermal decomposition process of municipal solid waste using TGA. *Waste Biomass Valoriz* 10:1679–1691
 37. Ibrahim WM, Hassan AF, Azab YA (2016) Biosorption of toxic heavy metals from aqueous solution by *Ulva lactuca* activated carbon. *Egypt J basic Appl Sci* 3:241–249
 38. Chrzanowska E, Gierszewska M, Kujawa J, Raszowska-Kaczor A, Kujawski W (2018) Development and characterization of polyamide-supported chitosan nanocomposite membranes for hydrophilic pervaporation. *Polymers (Basel)* 10:868
 39. Foroutan R, Mohammadi R, Peighambaroust SJ, Jalali S, Ramavandi B (2020) Application of nano-silica particles generated from offshore white sandstone for cadmium ions elimination from aqueous media. *Environ Technol Innov* 19:101031
 40. Youssef AM, Al-Awadhi MM, Akl MA (2014) Solid phase extraction and spectrophotometric determination of methylene blue in environmental samples using bentonite and acid activated bentonite from Egypt. *J Anal Bioanal Tech* 5:1
 41. Hayati-Ashtiani M (2012) Use of FTIR Spectroscopy in the Characterization of Natural and Treated Nanostructured Bentonites (Montmorillonites). Part. *Sci Technol* 30(6):553–564
 42. Koosha M, Hamed S (2019) Intelligent Chitosan/PVA nanocomposite films containing black carrot anthocyanin and bentonite nanoclays with improved mechanical, thermal and antibacterial properties. *Prog Org Coatings* 127:338–347
 43. David MK, Okoro UC, Akpomie KG, Okey C, Oluwasola HO (2020) Thermal and hydrothermal alkaline modification of kaolin for the adsorptive removal of lead (II) ions from aqueous solution. *SN Appl Sci* 2:1–13
 44. Foroutan R, Ehsandoost E, Hadipour S, Mobaraki Z, Saleki M, Mohebbi G (2016) Kinetic and equilibrium studies on the adsorption of lead by the chitin of pink shrimp (*Solenocera melanthro*). *Entomol Appl Sci Lett* 3:20–26
 45. Rahimi K, Mirzaei R, Akbari A, Mirghaffari N (2018) Preparation of nanoparticle-modified polymeric adsorbent using waste fuzes of mechanized carpet and its application in dye removal from aqueous solution. *J Clean Prod* 178:373–383
 46. Esvandi Z, Foroutan R, Peighambaroust SJ, Akbari A, Ramavandi B (2019) Uptake of anionic and cationic dyes from water using natural clay and clay/starch/MnFe₂O₄ magnetic nanocomposite. *Surf Interface* 21(1):100754
 47. García FE, Plaza-Cazón J, Montesinos VN, Donati ER, Litter MI (2018) Combined strategy for removal of Reactive Black 5 by biomass sorption on *Macrocystis pyrifera* and zerovalent iron nanoparticles. *J Environ Manage* 207:70–79
 48. Hajizadeh H, Peighambaroust SJ, Peighambaroust SH, Peressini D (2020) Physical, mechanical and antibacterial characteristics of bio-nanocomposite films loaded with Ag-modified SiO₂ and TiO₂ nanoparticles. *J Food Sci* 85:1193–1202
 49. Agnihotri S, Singhal R (2019) Effect of sodium alginate content in acrylic acid/sodium humate/sodium alginate superabsorbent

- hydrogel on removal capacity of MB and CV dye by adsorption. *J Polym Environ* 27:372–385
50. Ahmadi A, Foroutan R, Esmaeili H, Tamjidi S (2020) The role of bentonite clay and bentonite clay@MnFe₂O₄ composite and their physico-chemical properties on the removal of Cr(III) and Cr(VI) from aqueous media. *Environ Sci Pollut Res* 27:14044–14057. <https://doi.org/10.1007/s11356-020-07756-x>
 51. Khodaeimehr R, Peighambaroust SJ, Peighambaroust SH (2019) Preparation and characterization of corn starch/clay nanocomposite films: Effect of clay content and surface modification. *Starch-Stärke* 70(3–4):1700251
 52. Ebrahimi Y, Peighambaroust SJ, Peighambaroust SH, Karkaj SZ (2019) Development of Antibacterial Carboxymethyl Cellulose-Based Nanobiocomposite Films Containing Various Metallic Nanoparticles for Food Packaging Applications. *J Food Sci* 84(9):2537–2548
 53. Lee HS (1997) Biosorption of Cr, Cu and Al by Sargassum biomass. *Biotechnol Bioprocess Eng* 2:126–131.020–07756-x
 54. Al-Muhtaseb SA, El-Naas MH, Abdallah S (2008) Removal of aluminum from aqueous solutions by adsorption on date-pit and BDH activated carbons. *J Hazard Mater* 158:300–307
 55. Khattri S, Singh M (2009) Removal of malachite green from dye wastewater using neem sawdust by adsorption. *J Hazard Mater* 167:1089–1094
 56. Chaudhary S, Sharma J, Kaith BS, Yadav S, Sharma AK, Goel A (2018) Gum xanthan-psyllium-cl-poly(acrylic acid-co-itaconic acid) based adsorbent for effective removal of cationic and anionic dyes: adsorption isotherms, kinetics and thermodynamic studies. *Ecotoxicol Environ Saf* 149:150–158
 57. Kaushal S, Badru R, Kumar S, Kaur H, Singh P, (2018) Efficient removal of cationic and anionic dyes from their binary mixtures by organic–inorganic hybrid material. *J Inorg Organomet* 28:968–977
 58. Sabbagh F, Khatir NM, Karim AK, Nazari Z, Jaberi R (2019) Mechanical Properties and Swelling Behavior of Acrylamide Hydrogels using Montmorillonite and Kaolinite as Clays 7:211–219
 59. Sari A, Tuzen M (2009) Equilibrium, thermodynamic and kinetic studies on aluminum biosorption from aqueous solution by brown algae (*Padina pavonica*) biomass. *J Hazard Mater* 171:973–979
 60. Largitte L, Pasquier R (2016) A review of the kinetics adsorption models and their application to the adsorption of lead by an activated carbon. *Chem Eng Res Des* 109:495–504

Publisher's Note Springer Nature remains neutral with regard to jurisdictional claims in published maps and institutional affiliations.